Applied Physics A (2019) 125:185
https://doi.org/10.1007/s00339-019-2490-3

Applied Physics A
Materials Science & Processing

Effect of the $ZrCl_4$ static vaporiser system and deposition time on growth characteristics of chemical vapour deposited zirconium carbide layers

Saphina Biira[1] · Thulani T. Hlatshwayo[2] · Philip L. Crouse[3] · Hertzog Bissett[4] · Thabsile T. Thabethe[2] · Mbuso Mlambo[2] · Johan B. Malherbe[2]

Received: 13 August 2018 / Accepted: 11 February 2019

Abstract
ZrC layers were deposited from $ZrCl_4$–Ar–CH_4–H_2 gas mixture in a home-built vertical wall chemical vapour deposition system within the deposition time range 0.5–2.5 h. The flow behaviour of $ZrCl_4$ from the static vaporiser system to reaction chamber as a function of time was studied. To investigate the microstructure evolution and the growth characteristics of ZrC layers with deposition time, the growth rate, microstructure, morphology and composition were analysed. The layer thickness increased with deposition time all through; however, its growth rate increased up to 1.0 h and thereafter declined. The X-ray diffraction (XRD) analysis showed both ZrC and carbon peaks. The intensity of the carbon peaks followed a non-linear trend with deposition time. The average crystallite size and the number of crystallites per unit volume of the layers increased with deposition time. The orientation of crystallographic plane also varied with the deposition time. At short deposition times, the Raman spectra showed the acoustic and optic branches indicating that the ZrC deposited contained carbon vacancies. The D and G peaks of carbon increased as the deposition time increased, an indication of free carbon in the deposited layers. At short deposition times, the surface morphology of the layers was relatively flat and smooth. The particle size and agglomerations also increased with time.

1 Introduction

Zirconium carbide (ZrC) is a candidate material for use in high temperature nuclear reactors to replace or add to silicon carbide layer in the TRISO (tristructural isotropic) fuel particle [1]. This is because ZrC has been reported to possess very good physical, chemical, mechanical and irradiation-resistant properties [1–3]. ZrC either as a powder mixed with the fuel or as a thin layer on the fuel kernel has also been proposed for use as an oxygen getter in the UO_2 kernel TRISO fuel. The high oxidation potential of ZrC is perceived to act as a reducing agent for the oxygen generated from the fission process of UO_2. Therefore, shunning unfavourable oxidation reactions and reducing the formation of CO which are very detrimental more especially at high fuel burn-up levels [4]. One of the main obstacles that has hampered research to fully explore the properties of ZrC layers (for nuclear applications) is its manufacturing processes [3, 5]. Even though chemical vapour deposition (CVD) process has been identified as a method that can produce layers with high level of purity and low porosity [1, 3, 5], the deposition parameters (such as temperature, nature of precursors and ratios, pressure and time) and reactor geometry have to be optimised to achieve layers with the desired properties.

The CVD process of layers is achieved when gaseous precursors react chemically on the surface of a hot substrate [6, 7]. This means that when using solid precursors in the CVD process, the precursor has to be heated to generate vapour before it arrives at the substrate. The solid precursors are difficult to deliver to the reaction zone since most of them are not very volatile and may also clog the delivery channels [8].

✉ Saphina Biira
bsaphina@yahoo.co.uk

[1] Department of Physics, Busitema University, P.O Box 236, Tororo, Uganda

[2] Department of Physics, University of Pretoria, Pretoria 0002, South Africa

[3] Department of Chemical Engineering, University of Pretoria, Pretoria 0002, South Africa

[4] Applied Chemistry Division, The South African Nuclear Energy Corporation (Necsa), P.O Box 582, Pretoria 0001, South Africa

Published online: 15 February 2019

Therefore, an additional system (in this case, the vaporiser system) is usually included in the reactor system assembly to vaporise the solid precursors. This enhances precursor delivery and the chemical reaction of the precursor with others on the substrate surface. The vaporisation temperature should be high enough to achieve good partial pressure so as to maximize the precursor delivery into the reaction chamber. However, this temperature must be below its decomposition temperature, since this may lead to precursor delivery rates which are irreproducible. Furthermore, the type (e.g. static, impeller), geometry and orientation of the vaporiser system has been reported to influence the quantity delivered and the flow process of the zirconium salt to the reaction zone, and on the growth characteristics of the ZrC layer deposited [9–11]. Therefore, there is need to investigate how each type of the vaporizer influence the ZrC growth characteristics.

The CVD process involves a series of other processes, some of which occur concurrently and others in progression order [8]. Normally, the gaseous reactants are generated and then transported from the gas inlets through the boundary layer towards the hot substrate. The active precursors get adsorbed onto the surface of the hot substrate. The deposit and other by-products are produced by the chemical reaction at the gas–solid interface [1, 8]. The deposit then spreads out along the surface of a hot substrate producing the centre of crystallisation and developing the layer or coating. The gaseous by-products, including the unreacted gaseous precursor, are removed by the means of diffusion or convection [6, 12, 13]. A particular deposition time is required for these growth processes to deposit a material with the required properties. The choice for the appropriate deposition time is influenced by the type of layer being deposited, deposition temperature, nature of the precursors and other deposition parameters. Limited studies have been carried out to investigate the effect of deposition time [14] on the transportation of $ZrCl_4$ from the static vaporiser system into the reaction chamber and on the growth behaviour of ZrC layers. And yet certain tendencies during the deposition process (such as precursor delivery, growth rate) and structural evolution of CVD layers may be evidenced either in the early or later stages of the deposition process.

Xin et al. [14] investigated the effect of deposition time on microstructures and growth behaviour of ZrC coatings chemical vapour deposited at low pressure in a horizontal hot wall reactor using $ZrBr_4$ as zirconium source and C_3H_6 as carbon source, however, whether the vaporiser system used had an effect on the reported results was not mentioned. In this paper, the mass flow behaviour of $ZrCl_4$ from the static vaporiser system to the reaction chamber, ZrC growth rate, composition, morphology and microstructural properties of ZrC layers deposited in a vertical cold wall CVD system (with a static horizontal vaporiser system) at different deposition times are reported. Deposition time is a very important growth parameter that controls the layer quality, layer thickness and layer uniformity among others.

2 Experimental

2.1 Materials and methods

The CVD system with a static vaporiser system was used to grow ZrC layers at atmospheric pressure. The details of a vertical wall induction heated CVD reactor set up used and its description are given in ref [15, 16]. The ZrC source materials used were methane for carbon and $ZrCl_4$ powder. For each experimental run 6 g of $ZrCl_4$ powder were vaporised in a static vaporiser system to the required vapour pressure to optimise its flow into the reaction chamber. The $ZrCl_4$ vaporiser system consisted of an oven heated to 300 °C (just below its phase transition temperature of 331 °C) and a cylindrical steel vessel (24.6 cm long with inner diameter of 4.3 cm). The loaded cylindrical steel vessel was connected to the inlet pipes, and argon was allowed to sweep through freely. Figure 1 shows the physical layout of the $ZrCl_4$ vaporiser system.

Among the zirconium halides, $ZrCl_4$ is the frequently used zirconium source in the CVD of ZrC layers [3, 17, 18]. Thus, it was selected as a precursor for this study. The physical properties of $ZrCl_4$ are listed in Table 1. The gas flow rates at the inlet were maintained at 15 sccm, 862 sccm and 843 sccm for methane, hydrogen and argon, respectively. The gas glow rates were measured by manually controlling the flow meters. The argon gas was used to continuously swept $ZrCl_4$ vapour to the reaction chamber. Argon also played the role of stabilising the total reactor pressure and as well as a purge gas before the start of every deposition process. Hydrogen gas was used to provide a reducing and diluting environment for $ZrCl_4$ vapour. Clean polished circular graphite substrates were used for the ZrC deposition at 1400 °C at different deposition times ranging from 0.5 h to 2.5 h.

2.2 Characterisation

The crystal structural changes of as-deposited ZrC layers were analysed by an X-ray diffractometer (Bruker XRD D8 Advance) with a Cu K_α radiation source $\lambda = 0.15406$ nm. During XRD collection, the working potential and current were set at 40 kV and 40 mA, respectively. The values of 2θ were recorded between 15° and 125°. The as-deposited ZrC layers were also characterised by Raman spectroscopy. The Raman spectra were collected with a T64000 series II triple spectrometer system from HORIBA scientific, Jobin Yvon Technology. The Raman spectra were generated using argon/krypton laser with an excitation wavelength of

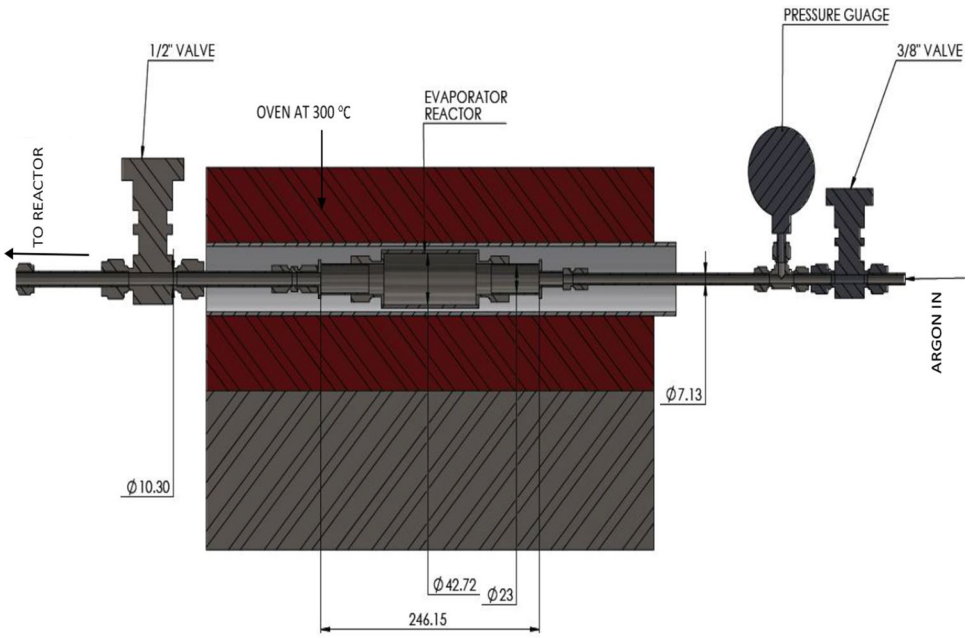

Fig. 1 The physical layout of the $ZrCl_4$ vaporiser system

Table 1 Physical properties of zirconium tetrachloride [19, 20]

Property	Specification
Appearance	White powder at room temperature
Molecular weight	233.03 g/mol at 15 °C
Density	2.80 (g/cm^3)
Transition temperature	331 °C
Latent heat of sublimation	4.54×10^5 J/kg at 331 °C
Specific gravity	2.805 g/cm^3 at 15 °C
Triple point temperature	473 (°C)
Triple point pressure	22.36 (bar)
Critical point temperature	504 (°C)
Critical point pressure	57.66 (bar)
Critical point volume	319 (ml/mol)

514 nm through an Olympus microscope with a 50× objective lens and laser power of 1.48 mW. The Raman spectra were acquired in the Raman shift range from 200 cm^{-1} to 1800 cm^{-1}. The surface morphology of the layers was characterised using a Zeiss Ultra Plus Field Emission Scanning Electron microscopy (FE-SEM) at an acceleration voltage of 1 kV. FE-SEM was also used to measure the thickness of the deposited ZrC layers by cross-sectional SEM analysis.

3 Results and discussion

3.1 Layer thickness and growth rate

The mass of $ZrCl_4$ powder and that of the vaporiser section (the cylindrical steel vessel) were measured before and after vaporisation to determine the mass loss and gain, respectively. This was done to ascertain the mass of the $ZrCl_4$ delivered in the reaction chamber from the static vaporiser at different deposition times. The coating thickness (x) was estimated using the mass increase of the substrate. The coating thickness was obtained using the equation; $x = \frac{M}{A\rho}$, where M is the mass of the coatings, A is the surface area of the substrate, $\rho$is the density of zirconium carbide (6.59 kg m^{-3}). The use of a constant zirconium carbide density value obviously introduces an error into the calculation of the growth rate (for this experiment, the error was assumed to be negligible).

Figure 2a shows the variation of the amount of $ZrCl_4$ used during the ZrC deposition process using the $ZrCl_4$ static vaporiser. Figure 2b shows the variation of layer thickness and the growth rate (the coating thickness per unit time) of ZrC layers at various deposition times. Short deposition time showed an accelerated layer thickness growth (i.e. fast growth from 0.5 h to 1.0 h and slow growth from 1.0 h to 2.5 h); see the growth rate curve in Fig. 2b. Even though the gas feed lines were wrapped with an electrical heat tracing tape, there was still a tendency of $ZrCl_4$ accumulating along the vaporiser feed line towards the reaction chamber. This was evidenced by the increase in mass of the vaporiser with deposition time which reduced the mass delivery rate of $ZrCl_4$ to the reaction chamber (see Fig. 2a). This resulted in the slowing down of the rate of the chemical reaction which is proportional to the ZrC layer growth rate. Also the continuous flow of argon ($ZrCl_4$ carrier gas) reduces the amount of $ZrCl_4$ vapour in the vaporiser with time. It is important to note

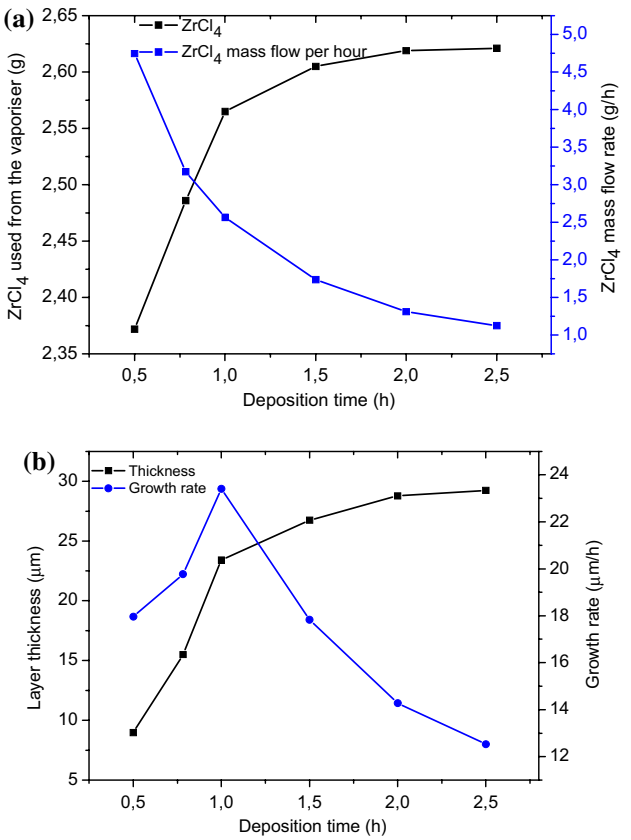

Fig. 2 **a**: Variation of the amount of $ZrCl_4$ used during the ZrC deposition process using the $ZrCl_4$ static vaporiser. **b** Influence of deposition time on layer thickness and growth rate

that for each experiment, equal amount of $ZrCl_4$ powder (i.e. 6.0 g) was loaded in the vaporiser system.

3.2 XRD structural and phase analysis

The XRD patterns of ZrC layers deposited at 0.5 h, 1.0 h, 1.5 h, 2.0 h and 2.5 h using the static vaporiser are shown in Fig. 3. The diffraction patterns revealed mainly ZrC peaks and traces of free carbon when matched with the standard date file number ICDD ZrC: 03-065-8833 and ICDD C: 00-008-0415, respectively. The ZrC diffraction peaks present were indexed within a cubic rock-salt (NaCl) structure type with Miller indices of (111), (200), (220), (311), (222), (400), (331), (420), (422) and (511) corresponding to $2\theta°$ at about 32.9, 38.3, 55.2, 65.9, 69.2, 81.9, 91.2, 94.3, 106.8 and 116.8, respectively (see Fig. 3). The carbon phase present was found to be hexagonal graphite with its prominent reflections indicated by C at (0002) with $2\theta°$ at about 26.5, respectively. To study the trend and behaviour of this carbon phase with deposition time, Raman spectroscopy was employed (since it is more sensitive to structural changes than XRD), see Sect. 3.4.

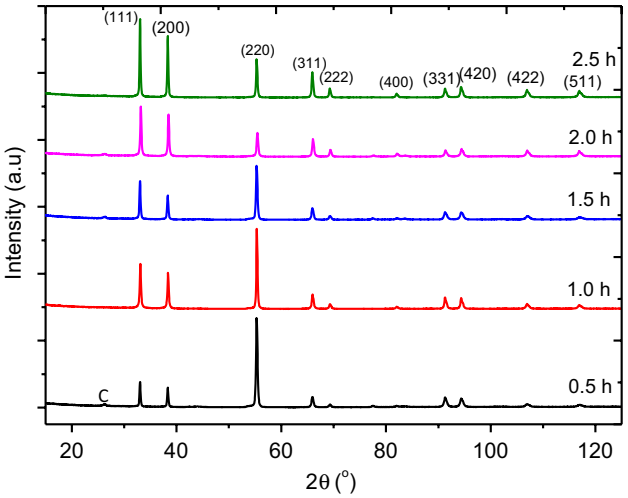

Fig. 3 XRD pattern of ZrC layers deposited at different deposition times

The ZrC diffraction patterns were characteristic of well-defined sharp Bragg's peaks. This indicated that the ZrC layers deposited at all deposition times possessed a good degree of crystallinity. Figure 3 also show that changes in deposition time had an effect on peak intensity and consequently on the orientation of the planes as indicated in Fig. 4. The preferred orientation as deduced from the texture coefficient (determined from the Harris method) [21, 22] revealed that the diffraction plane (220) had the preferred orientation at all deposition times. However, its texture coefficient values reduced from 3.32 to 1.02 as deposition time was increased from 0.5 h to 2.5 h and as the $ZrCl_4$ mass flow rate reduced from 4.74 g/h to 1.13 g/h. Whereas the diffraction planes (111) (200), (311) and (222) were randomly oriented (i.e.

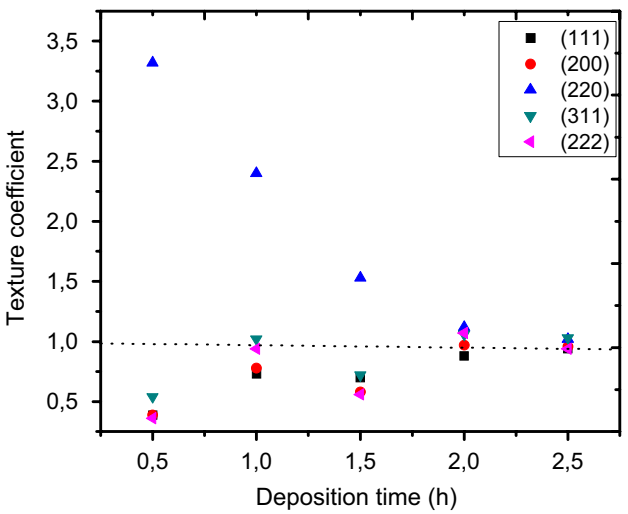

Fig. 4 Variation of texture coefficient with deposition time

the value of their texture coefficient was less than one) at all deposition times and $ZrCl_4$ mass flow rates. The texture coefficient values of the randomly oriented planes increased gradually with deposition time. For example, the texture coefficients of planes (111) and (200) increased from 0.39 to 0.96 with increase in deposition time/reduction in $ZrCl_4$ mass flow rate.

At the very early stages of nucleation, crystallites are randomly oriented [23]. When the layer thickness increases, crystallites with the fastest growing crystallographic planes normal to the substrate envelope the other crystallites. The crystallographic planes that are more exposed determines the final orientation of the deposited layer (evolutionary selection rule) [23, 24]. It is also important to note that crystallites grow such that they minimise the sum of surface energy and strain energy in an attempt to attain equilibrium conditions. Since these energies vary from one crystallographic plane to another, orientation of planes is not always the same. In our case, we observed small crystallite at short deposition time (as depicted by SEM images in Sect. 3.5). The reason for this was the high growth rate (contributed to by the high $ZrCl_4$ mass flow rate at short deposition time) of the ZrC layer, which introduced defects into the layer. According to the step-flow model of crystal growth [25], these defects act as growth points for new (small) crystallites. This favoured the growth of larger crystals as deposition time increased and $ZrCl_4$ mass flow rate decreased. Crystal growth is a kinetic process which requires both temperature and time therefore; as time is increased the crystallites will grow into larger ones. This is due to continued diffusion of the ZrC molecules into each other (just like during annealing). Small crystallites have high surface energies compared to large crystallites. This favours the growth of high energy crystallographic planes, thereby increasing the areas of the low energy planes in line with Wulf's law [26]. In addition, due to their high surface energies, the small crystals get absorbed into the larger crystals (Ostwald ripening) to minimise the total surface energy. This parasitic growth of the crystals maximises the areas of crystal planes with lower surface energies also in line with Wulf's law. This explains the reason why (220) was the initial preferred orientation and the reason why its texture coefficient value (as observed in Fig. 3) gradually decreased with increasing deposition time. Consequently, there was a gradual increase in the texture coefficient values of the low energy planes (111) and (200).

It is also important to note that the deposition in this study was conducted at high temperatures (1400 °C). It has been reported that at 1400 °C the CVD growth process of ZrC is mass transport controlled [16]. Kajikawa et al. [27] reported that the most densely packed planes (i.e. (111)) grow faster among other crystallographic planes in the surface reaction controlled regime, whereas the plane (220) grows faster in the adsorption controlled regime; supporting the results obtained in this study.

3.3 Microstructure evolution

The average crystallite size (D) was calculated from Scherrer's formula given by the following equation:

$$D = \frac{0.94\lambda}{\beta \cos\theta}, \tag{1}$$

where θ is the Bragg angle of diffraction, λ is the wavelength of the X-ray used and β is the peak broadening at full-width at half-maximum [21]. The average crystallite size of the as-deposited ZrC layers was found to increase from 27.8 nm to 32.3 nm as the deposition time was increased from 0.5 h to 2.5 h as indicated in Fig. 5. The reasons for this crystal size increase were discussed in Sect. 3.2.

The degree of clustering of the crystallites in the layer, the size and shape of the crystallites are among the factors that influence the number of crystallites per unit volume in the layer. Therefore, the number of crystallites per unit volume (N) of ZrC layers was determined from the following equation:

$$N = \frac{x}{D^3}, \tag{2}$$

where D is the average crystallite size and x is the layer thickness [28, 29]. From Fig. 5, it can be seen that the number of crystallites per unit volume increased with increase in the time of deposition. This is an indication that the amount of $ZrCl_4$ delivered per unit time in the reaction chamber also affects the number of crystallites per unit volume of the layer deposited. One would expect the number of crystallites per unit volume to decrease with increase in crystallite size. However, this was not the case, since increasing the layer

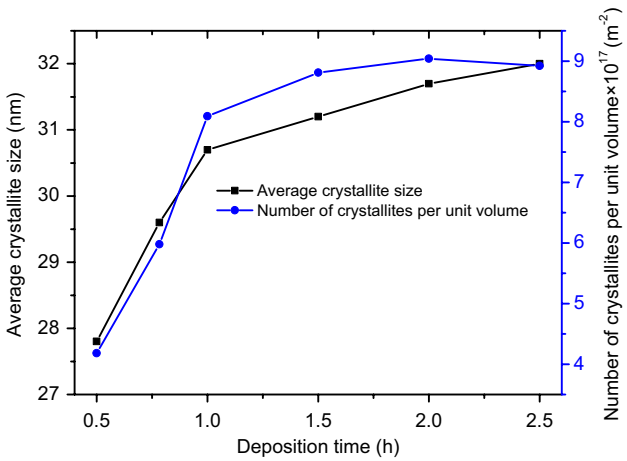

Fig. 5 Dependence of average crystallite size and number of crystallites per unit volume on deposition time

thickness increases the volume and therefore more crystallites can be occupied. The above result suggests that the layer thickness grew faster than the crystallite size did.

3.4 Raman analysis

Raman spectroscopic analysis was used as one of the effective means to establish the purity and composition of the deposited ZrC layers. Raman spectroscopic analysis produces a characteristic spectrum for materials depending on the vibrational modes of their molecules [30]. Figure 6 shows the Raman spectra acquired at room temperature for samples deposited at different deposition times. ZrC possesses a crystal structure like that of NaCl. Stoichiometric compounds with a NaCl structure have all their atoms laying at the sites of inversion symmetry and therefore do not allow first-order Raman scattering [31, 32]. This means that stoichiometric ZrC is not Raman active and hence no ZrC Raman peak can be detected. However, within the measured spectral range, the deposited ZrC layers revealed some peaks at Raman shift of about 210 cm^{-1}, 290 cm^{-1}, 522 cm^{-1}, 625 cm^{-1}, 1350 cm^{-1} and 1580 cm^{-1} (see Fig. 6 and the figure inserted). This means that the deposited ZrC layers are ideally not stoichiometric or contains some level of impurities. It has been reported that ZrC primitive cells have 2 atoms with 6 vibrational modes, half of which are acoustic and the other half are optical modes [33]. Kim et al. [31] reported that ZrC Raman spectrum with peaks at around 210 cm^{-1} and 280 cm^{-1} representing acoustic branches and the Raman peaks at 540 cm^{-1} and 600 cm^{-1} representing optical branches due to the presence of carbon vacancies in the ZrC structure. The reason for this is that the vacancies in the ZrC structure interrupts the local symmetry, permitting the defect-induced Raman scattering to be detected [31, 34]. This means that at low deposition times, there were more carbon vacancies in the ZrC structure (i.e. we have a sub-stoichiometric ZrC hereby represented by ZrC_{1-x}). As was discussed in Sect. 3.2, at low deposition times, the growth rate of the ZrC layer was very high. This high growth rate introduced more defects, including carbon vacancies, into the layer. As the deposition time was increased from 1.0 h to 2. 5 h, the peaks at about 210, 290, 522 cm^{-1} and 625 cm^{-1} reduced, instead the free carbon peaks originating from carbon inclusions in the ZrC matrix at around 1350 and 1580 became more prominent. This means that number of carbon vacancies decreased with a growth in free carbon inclusions. The carbon peaks are evidenced by the presence of D and G bands. The D-band is associated with defects in graphitic materials. The G band is associated with in-plane vibrations of C–C bonds and is a measure of graphitization or degree of metallicity of graphitic materials [35, 36].

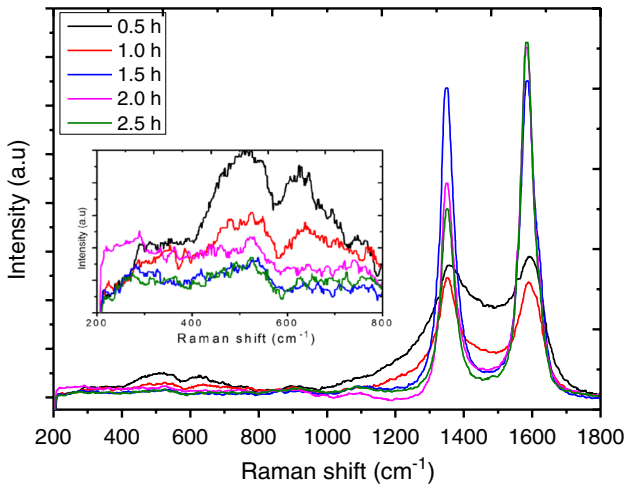

Fig. 6 Raman spectroscopy analysis of ZrC layers at different deposition times

It was observed that at 0.5 h and 1 h the D and G peaks are broad as can be seen from the FWHM values in Table 2 also illustrated by Fig. 7. This shows that at short deposition time, there is poor crystallisation of the free carbon which improves as the deposition time is increased in line with the crystal growth model discussed in Sect. 3.2. At 0.5 h and 1.0 h, the free carbon is more of amorphous type than graphitic type because the 1500 cm^{-1} Raman peak shows a broad band (see Fig. 7) which is comparable to amorphous sp^2 bonded carbon [37]. Also as the deposition time increased from 0.5 h to 2.5 h, there was a shift to the left of both the D and G bands from 1359 to 1348 cm^{-1} and from 1590 to 1581 cm^{-1}, respectively.

There was an increase in intensities of G peaks and a non-linear trend in intensities of D peak as the deposition time was increased as observed from Fig. 7. This implies that the

Table 2 Raman analysis data of the D and G peaks evolution in ZrC layers deposited at different times

Deposition time (h)	Peak position (cm^{-1})		FWHM (cm^{-1})		Intensity (a.u)		I_D/I_G
	D	G	D	G	D	G	
0.5	1358.21	1589.74	200.35	157.41	1.13	1.20	0.94
1.0	1349.35	1588.56	92.11	92.64	1.04	1.00	1.04
1.5	1347.58	1583.83	47.26	57.02	2.71	2.77	0.98
2.0	1347.58	1581.47	47.63	46.22	1.87	3.04	0.62
2.5	1349.35	1581.47	46.74	45.19	1.63	3.06	0.53

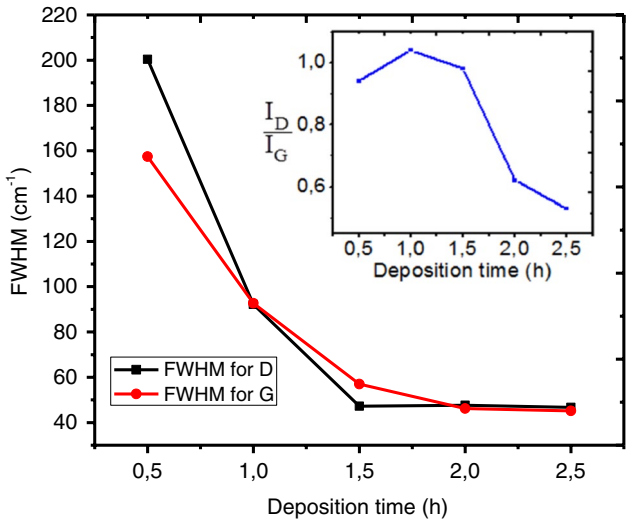

Fig. 7 Variation of FWHM of D and G carbon peaks with deposition time. The insert indicates the variation of the I_D/I_G with time

quantity of free carbon co-deposited did not increase linearly with deposition time as evidenced in XRD spectrum (in our next study, suitable techniques will be used to quantify this free carbon content). The non-linear trend in the quantity of the co-deposited carbon may be due to a number of complex competing reaction and crystal growth mechanisms. For instance, CH_4 and $ZrCl_4$ have different decomposition rates and activation energies. At short deposition time, all the decomposed carbon (free carbon/atomic carbon) might have not reacted with $ZrCl_4$ to form ZrC. In this case, free carbon and the ZrC structure which is not fully formed are observed, as already mentioned. The free carbon is actually more of amorphous at short deposition time (see Fig. 6). There is also decreased flow of $ZrCl_4$ as deposition time is increased and a constant supply of methane, the source for the carbon atoms, to the reaction surface as explained in [38]. This might have enhanced the growth rate of the carbon inclusions which became more graphitic with deposition time.

Apart from the deposition time of 0.5 and 1 h where the nature of the free carbon appear amorphous, consider the deposition time from 1.5 to 2.5 h in which the intensity of G peak increased, whereas that of the D peak decreased as the deposition time increased. This may be due to the improved sample crystal structure refining of the carbon material with deposition time. In line with this argument, the values of I_D/I_G given in Table 2 decrease with increase in deposition time. The I_D/I_G ratio is a measure of the degree of defects in the structure of carbon materials. As was mentioned above, the G peak is a result of in-plane vibrations of sp^2 bonded carbon atoms, whereas the D peak is due to out of plane vibrations attributed to the presence of structural defects [35, 39]. This means that I_D/I_G forms a connection with sp^3/sp^2 ratio. So as the deposition time was increased there was increased transition from sp^3 material to sp^2 material, meaning that there was reduction in the defects in the structure of the carbon material. So the free carbon in the deposited layers becomes more graphitic. This is supported by the corresponding decrease in the FWHM peak widths of the G peak in Table 2.

3.5 Surface morphology

Figure 8 shows the surface morphology of ZrC layers deposited at 1400 °C at different deposition times. It was observed that the morphology of the ZrC varied with deposition time. At deposition time of 0.5 h, the ZrC layer surface is composed of discrete uniform particles and a few protrusions. At 1 h, the small particles started to aggregate and the surface became rough. When the deposition time was further increased (1.5 h, 2 h and 2.5 h), the particles increased in size and became more agglomerated. There was a tendency of particles piling on top of the other, which may be explained by preferential thermophoretic deposition of particles [27].

Even though the average crystallite size calculated from the XRD using Scherer's equation increased with deposition time just as size of crystals observed from the SEM micrographs, they may not easily be compared because of the coalescence of crystals into aggregates. Further still, SEM only probes near surface region of the sample compared to the XRD which probes much deep inside the material.

4 Conclusion

ZrC layers were deposited on graphite substrates by chemical vapour deposition technique at 1400 °C at different deposition times. The $ZrCl_4$ vapour was generated in horizontal static vaporiser system. Our findings indicated that the static $ZrCl_4$ vaporiser and the duration of $ZrCl_4$ flow to the reaction chamber had an effect on the quantity of $ZrCl_4$ delivered into the reaction chamber. The amount of $ZrCl_4$ entering the reaction chamber declined with increase in the deposition time. This may be due to the continuous accumulation of $ZrCl_4$ in the vaporiser feed line and the continuous blowing of argon. At short deposition time, ZrC layer thickness increased faster than at long deposition time. Consequently, there was an increase in the ZrC layer growth rate up to 1 h, thereafter it declined. Further characterisation of the ZrC layers was carried out using XRD, SEM and Raman spectroscopy techniques. XRD analysis revealed the polycrystalline face-centred structure of ZrC layers and some traces of free carbon. The preferred orientation of the diffraction planes was (220), and its texture coefficient value decreased as deposition time increased.

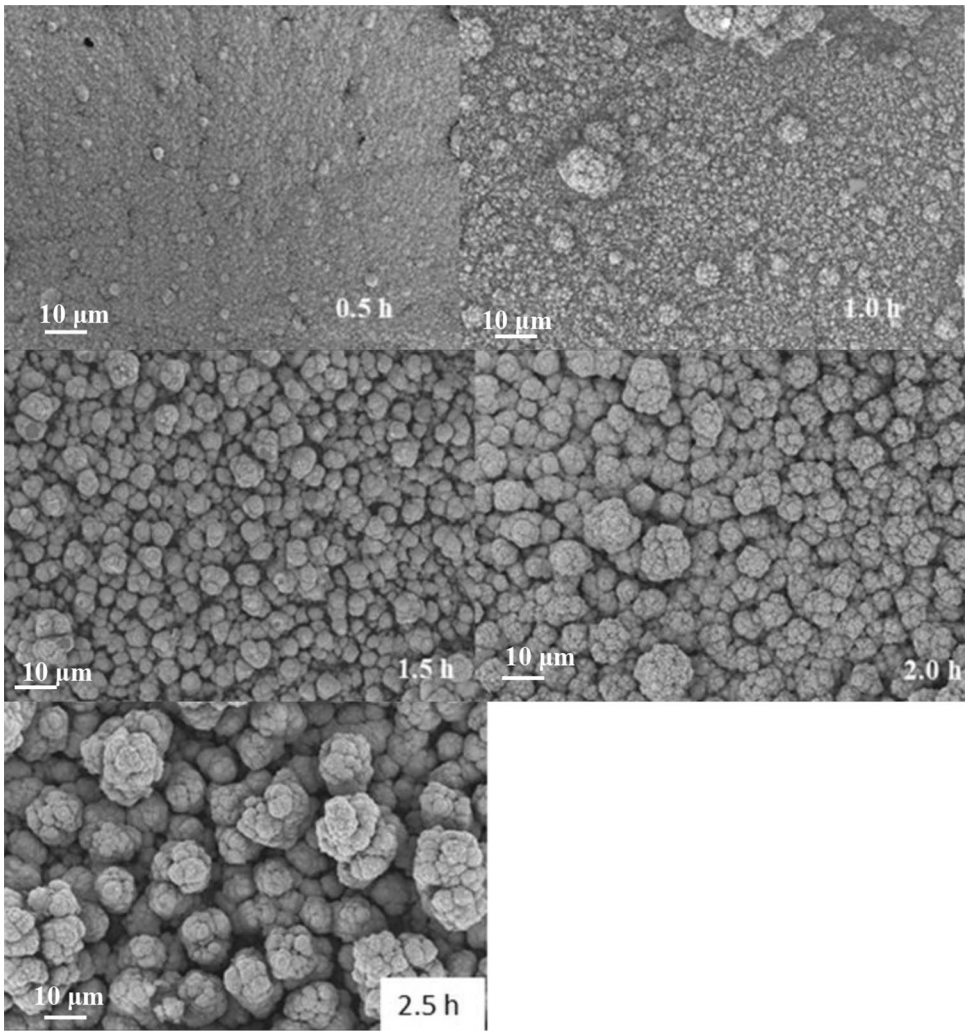

Fig. 8 The evolution of ZrC surface morphology with deposition time

The planes (111) and (200) had no preferred orientation but their texture coefficient values increased with deposition time. The crystallite size grew from 27.8 nm to 32.3 nm as the deposition time increased from 0.5 h to 2.5 h. The number of crystallite per unit volume increased with deposition time due to increased layer thickness. The Raman spectra revealed the presence of free carbon, whose quantity followed a non-linear trend with deposition time. At the beginning, the free carbon was amorphous, but its level of crystallisation improved with deposition time. The deposition time had an influence on the surface morphology as well. At the shorter deposition times, the surfaces of the ZrC layers composed of discrete uniform particles and a few protrusions. As the deposition time increased, particle increased in size, and agglomeration of particles also increased.

Acknowledgements Necsa and the Department of Science and Technology of South Africa through the Nuclear Materials Development Network of the Advanced Metals Initiative are highly appreciated for the provision of funding, laboratory space and experimental materials. The funding from Busitema University, the African Union and the University of Pretoria are highly acknowledged.

References

1. Y. Katoh, G. Vasudevamurthy, T. Nozawa, L.L. Snead, Properties of zirconium carbide for nuclear fuel applications. J. Nucl. Mater. **441**, 718–742 (2013)
2. R.W. Harrison, W.E. Lee, Processing and properties of ZrC, ZrN and ZrCN ceramics: a review. Adv. Appl. Ceram. **115**, 294–307 (2016)
3. Y. Wang, Q. Liu, J. Liu, L. Zhang, L. Cheng, Deposition mechanism for chemical vapor deposition of zirconium carbide coatings. J. Am. Ceram. Soc. **91**, 1249–1252 (2008). https://doi.org/10.1111/j.1551-2916.2007.02253.x
4. L.L. Snead, Y. Katoh, S. Kondo, Effects of fast neutron irradiation on zirconium carbide. J. Nucl. Mater. **399**, 200–207 (2010)
5. A.J. Woo, G. Bourne, V. Craciun, D. Craciun, R.K. Singh, Mechanical properties of ZrC thin films grown by pulsed laser deposition. J. Optoelectron. Adv. Mater. **8** (1), 20–23 (2006)

6. K.L. Choy, Chemical vapour deposition of coatings. Prog. Mater Sci. **48**, 57–170 (2003)
7. J. Park, T.S. Sudarshan, *Chemical Vapor Deposition* (ASM International, Chicago, 2001)
8. H.O. Pierson, *Handbook of Chemical Vapor Deposition: Principles, Technology and Applications*, 2nd edn. (William Andrew, New York, 1999)
9. C.M. Hollabaugh, R.D. Reiswig, P. Wagner, L. Wahman, R.W. White, A new method for coating microspheres with zirconium carbide and zirconium carbide-carbon graded coats. J. Nucl. Mater. **57**, 325–332 (1975). https://doi.org/10.1016/0022-3115(75)90217-2
10. T.C. Wallace, Chemical vapor deposition of ZrC in small bore carbon-composite tubes. No. LA-UR-73-692. Los Alamos Scientific Laboratory, New Mexico, USA (1973)
11. A.R. Driesner, E.K. Storms, P. Wagner, T.C. Wallace, High temperature-low density ZrC insulators made by chemical vapor deposition. No. LA-UR-73-804; CONF-731017-2. Los Alamos Scientific Laboratory, New Mexico, USA (1973)
12. M. Ohring, *Materials Science of Thin Films*, 3rd edn. (Academic press, London, 2002)
13. J.L. Vossen, W. Kern, *Thin Film Processes II* (Academic press, San Diego, 1991)
14. M. Xin, L. Yong, M. Min, H. Haifeng, H. Xinbo, Q. Xuanhui, C. Si'an, Effect of deposition time on microstructures and growth behavior of ZrC coatings prepared by low pressure. J Wuhan Univ Technol Mater Sci Ed **32**, 284–288 (2017). https://doi.org/10.1007/s11595-017-1593-y
15. S. Biira, P.L. Crouse, H. Bissett, B.A.B. Alawad, T.T. Hlatshwayo, J.T. Nel, J.B. Malherbe, Optimisation of the synthesis of ZrC coatings in a radio frequency induction-heating chemical vapour deposition system using response surface methodology. Thin Solid Films **624**, 61–69 (2017). https://doi.org/10.1016/j.tsf.2017.01.018
16. S. Biira, B.A.B. Alawad, H. Bissett, J.T. Nel, T.P. Ntsoane, T.T. Hlatshwayo, P.L. Crouse, J.B. Malherbe, Influence of the substrate gas-inlet gap on the growth rate, morphology and microstructure of zirconium carbide films grown by chemical vapour deposition. Ceram. Int. **43**, 1354–1361 (2017). https://doi.org/10.1016/j.ceramint.2016.10.092
17. Q. Liu, L. Zhang, L. Cheng, Y. Wang, Morphologies and growth mechanisms of zirconium carbide films by chemical vapor deposition. J Coatings Technol Res **6**, 269–273 (2009)
18. J.H. Park, C.H. Jung, D.J. Kim, J.Y. Park, Temperature dependency of the LPCVD growth of ZrC with the ZrCl4-CH4-H2 system. Surf Coatings Technol **203**, 324–328 (2008)
19. P. Patnaik, *Handbook of Inorganic Chemicals* (McGraw-Hill, New York, 2003)
20. Y.M. Jung, M.K. Gyeong, L. Moonyong, Measurement of bubble point pressures of zirconium and hafnium tetrachloride mixture for zirconium tetrachloride purification process. Int J Chem Eng Appl **3**, 427–429 (2012)
21. B.D. Cullity, S.R. Stock, *Elements of X-ray Diffraction*, 1st edn. (Addison-Wesley Publishing company Inc, Massachusetts, 1956)
22. J.P. Enríquez, X. Mathew, Influence of the thickness on structural, optical and electrical properties of chemical bath deposited CdS thin films. Sol Energy Mater Sol Cells **76**, 313–322 (2003)
23. Y. Kajikawa, N. Sugura, K. Hirosha, Mechanisms controlling preferred orientation of chemical vapor deposited polycrystalline films. Solid State Phenom **93**, 411–418 (2003). https://doi.org/10.4028/www.scientific.net/SSP.93.411
24. Y. Kajikawa, Texture development of non-epitaxial polycrystalline ZnO films. J. Cryst. Growth **289**, 387–394 (2006). https://doi.org/10.1016/j.jcrysgro.2005.11.089
25. W.-K. Burton, N. Cabrera, F.C. Frank, The growth of crystals and the equilibrium structure of their surfaces. Philos. Trans. R Soc. Lond. A Math. Phys. Eng. Sci. **243**, 299–358 (1951)
26. C.-C. Liu, J.-H. Huang, C.-S. Ku, S.-J. Chiu, J. Ghatak, S. Brahma, C.-W. Liu, C.-P. Liu, K.-Y. Lo, Crystal orientation dynamics of collective zn dots before preferential nucleation. Sci Rep **5**, 12533 (2015). https://doi.org/10.1038/srep12533
27. Y. Kajikawa, N. Suguru, K. Hiroshi, Preferred orientation of chemical vapor deposited pollycrystalline silicon carbide films. Chem Vap Depos **8**, 99–104 (2002)
28. S. Prabahar, M. Dhanam, CdS thin films from two different chemical baths-structural and optical analysis. J. Cryst. Growth **285**, 41–48 (2005). https://doi.org/10.1016/j.jcrysgro.2005.08.008
29. S.A. Jassim, A.A. Rashid, A. Zumaila, G. Abdella, A. Al, Influence of substrate temperature on the structural, optical and electrical properties of CdS thin films deposited by thermal evaporation. Results Phys. **3**, 173–178 (2013). https://doi.org/10.1016/j.rinp.2013.08.003
30. K.S. Munir, M. Qian, Y. Li, D.T. Oldfield, P. Kingshott, D.M. Zhu, C. Wen, Quantitative analyses of MWCNT-Ti powder mixtures using raman spectroscopy: the influence of milling parameters on nanostructural evolution. Adv. Eng. Mater. **17**, 1660–1669 (2015). https://doi.org/10.1002/adem.201500142
31. D. Kim, Y.B. Chun, M.J. Ko, H. Lee, M. Cho, J.Y. Park, W. Kim, Microstructure evolution of a ZrC coating layer in TRISO particles during high-temperature annealing. J. Nucl. Mater. **479**, 93–99 (2016). https://doi.org/10.1016/j.jnucmat.2016.06.024
32. S. Pellegrino, L. Thomé, A. Debelle, S. Miro, P. Trocellier, Radiation effects in carbides: TiC and ZrC versus SiC. Nucl. Inst. Methods Phys. Res. B **327**, 103–107 (2014). https://doi.org/10.1016/j.nimb.2013.11.046
33. L. Hui, L. Zhang, Q. Zeng, H. Ren, K. Guan, Q. Liu, L. Cheng, First-principles study of the structural, vibrational, phonon and thermodynamic properties of transition metal. Solid State Commun. **151**, 61–66 (2011). https://doi.org/10.1016/j.ssc.2010.08.034
34. H. Wipf, M.V. Klein, W.S. Williams, Vacancy-induced and two-phonon Raman scattering in ZrCx, NbCx, HfCx, and TaCx. Phys. Status Solidi **108**, 489–500 (1981)
35. A.C. Ferrari, J. Robertson, Interpretation of Raman spectra of disordered and amorphous carbon. Phys. Rev. B **61**, 14095 (2000)
36. E. Petrova, S. Tinchev, P. Nikolova, Interference effects on the ID/IG ratio of the Raman spectra of diamond-like carbon thin films. arXiv:1112.0897 (2011)
37. M. Patel, C.L.A. Ricardo, P. Scardi, P.B. Aswath, Morphology, structure and chemistry of extracted diesel soot—Part I: Transmission electron microscopy, Raman spectroscopy, X-ray photoelectron spectroscopy and synchrotron X-ray diffraction study. Tribol Int **52**, 29–39 (2012)
38. S. Biira, P.L. Crouse, H. Bissett, T.T. Hlatshwayo, E.G. Njoroge, J.T. Nel, T.P. Ntsoane, J.B. Malherbe, The role of ZrCl4 partial pressure on the growth characteristics of chemical vapour deposited ZrC layers. Ceram. Int. **43**, 15133–15140 (2017). https://doi.org/10.1016/j.ceramint.2017.08.042
39. A.C. Ferrari, J. Robertson, Resonant Raman spectroscopy of disordered, amorphous, and diamondlike carbon. Phys. Rev. B **64**, 075414 (2001). https://doi.org/10.1103/PhysRevB.64.075414